PCCP

Accepted Manuscript

Effect of electric field during annealing of organic light emitting diodes for improving its On/Off ratio

Rahul K. Sharma[a,b], Monica Katiyar[a,b], I. V. Kameshwar Rao[b#], K. N. Narayanan Unni[c] and Deepak[a,b*]

[a]Department of Materials Science and Engineering, Indian Institute of Technology Kanpur, Kanpur 208016, India

[b]Samtel Centre for Display Technologies, Kanpur, Kanpur 208016, India

[c]Photosciences and Photonics Section, Chemical Sciences and Technology Division, CSIR-National Institute for Interdisciplinary Science and Technology, Trivandrum 695019, India

Currently with Nanyang Technological University, Singapore.

* Corresponding author: Tel.: +91 512 2597353, E-mail address: saboo@iitk.ac.in (Deepak).

Abstract

If an organic light emitting diode is to be used as part of a matrix addressed array, it should exhibit low reverse leakage current. In this paper we present a method to improve the on/off ratio of such a diode by simultaneous application of heat and electric field post device fabrication. A green OLED with excellent current efficiency was seen to be suffering from poor on/off ratio of 102. After examining several combinations of annealing along with the application of a reverse bias voltage, the on/off ratio of the same device could be increased by three orders of magnitude, specifically when the device was annealed at 80^{o}C under reverse bias (-15V) followed by slow cooling also under the same bias. Simultaneously, the forward characteristics of the device were relatively unaffected. The reverse leakage in OLED is mainly due to injection of minority carriers in hole transport layer (HTL) and electron transport layer (ETL); in this case, of holes in Tris-(8-hydroxyquinoline)aluminum(Alq_3) and electrons in 4,4',4''-Tris(N-3-methylphenyl-N-phenylamino)triphenylamine (m-MTDATA). Hence, to investigate these layers adjacent to the electrodes, we fabricated their single layer devices. The possibility of bulk traps present adjacent to electrodes providing states for injection was ruled out after estimating the trap density both before and after the reverse biased annealing. The temperature independent current in reverse bias ruled out possibility of thermionic injection. The origin of the reverse bias current is attributed to availability of interfacial hole levels in Alq_3 at the cathode work function level in the as-fabricated device; the suppression of the same being attributed to the fact that these levels in Alq_3 are partly removed after annealing under an electric field.

Introduction

Organic Light Emitting Diodes (OLEDs) are now being used as information displays in several consumer electronics products. During the past few years display technology has seen a dramatic improvement in terms of display size, display quality and luminance efficiency. The currently available smart phone displays have huge pixel density along with very high brightness and long lifetime. Basic challenges before the display industry are to improve the frame rates, device stability, display quality and the yield. It can be noted that in OLED based displays the performance of the OLED device has a direct bearing on all the above aspects and thus improving the performance of the OLED device becomes critically important. This has been attempted by using highly efficient phosphorescent materials, introducing doped transport layers and by using outcoupling techniques[1-3].

Reverse leakage current is an important performance indicator of an OLED. It becomes very critical in applications such as passive matrix (PM) OLED displays, where a leakage current can lead to cross-talk in displays as shown by Gu and Forrest[4]. There have been some early efforts to understand the origin of the reverse leakage current in OLEDs. Reverse leakage current has been viewed as originating due to the roughness of the indium tin oxide (ITO) anode and it has been shown that the devices fabricated on rough ITO films showed higher reverse leakage current[5]. In a polyvinylcarbazole (PVK) based OLED, the reverse leakage current was suppressed by adding a Alq_3 film between the emitter and the cathode as it prevented hole injection into PVK from the cathode[6]. Perimeter leakage currents have been proposed as the reason for reverse leakage current in polymer LEDs[7].

It is found that the mid-gap aggregate states give rise to negative differential resistance in the I-V characteristics of a peryelenetetracarboxilicdianhydride (PTCDA) film and this can be removed by exposing the film to UV radiation because the photo-excited carriers fill up the states. Such midgap states may give rise to leakage current under reverse bias conditions[8].

Impedance spectroscopy has been used to show that high leakage currents resulted from additional current paths due to possible lateral conduction of the interlayers[9]. The reverse leakage current has been shown to decrease by one order of magnitude if the cathode was deposited at 77K. Reduced damage on the metal contact and organic film interface have been cited as the reasons for the improved performance[10]. Thus origin of reverse bias leakage current can be explained by two mechanisms (i) field-emission tunneling from metal to semiconductor and (ii) trap assisted leakage current[11]. The structural disorders in materials, chemical and morphological defects and impurities present in thin films lead to the presence of trap states in the semiconductor, which are responsible for the deterioration of the device performance. Lot of effort is put on costly purification processes to ensure the quality of materials. However, the possibility of controlling the device properties by post-fabrication treatments other than simple annealing has not been explored well.

Controlled heating has been found to enhance the device performance in an Alq_3 based device. With annealing, the electron only devices showed improvement and the hole only device showed no improvement[12]. Selective thermal heating has been useful to improve the properties, especially annealing the Al layer, which indicated that the electron injection was otherwise poor[13]. Annealing at 70^{o}C for 5 hours helped improving the performance of a Alq_3 based OLED[14]. It is also reported that the mild heating at 70°C might have modified and enhanced the bonding at the interfaces of organic layer, resulting in decreased turn-on voltage, less leakage current, higher luminescence, and longer lifetime in the case of an Alq_3 based OLED[15]. The improvement in a rubrene based device upon annealing is attributed to the change in the interface characteristics and carrier diffusivity[16]. Properties of polyfluorene OLEDs are also seen to be affected by annealing[17]. The thermal treatment is seen to result in the formation of an interfacial layer between the organic film and the aluminum cathode, improving the injection of electrons from cathode in a polymer LED[18].

In another report, the stabilization of intrinsic polymorphism of the organic film induced by thermal energy and the morphology being subsequently modified to a lowest energetic configuration have been suggested to be the reasons for improved performance upon thermal annealing in a Alq_3 based OLED[19]. The crystallinity and change of roughness of each layer in an OLED with Alq_3 as the emitting layer at various heat-treatment steps have been studied by Yoon et al.[20]. Surface morphology change and subsequent better contact of organic/metallic layers upon annealing may result in increased injection current. This fact has been corroborated by the increase in performance of Alq_3 based OLEDs fabricated at different substrate temperatures[21].

Application of a suitable electrical field has also seen to affect the properties of OLEDs. Upon electrical annealing a conjugated dendrimer based OLED has shown reduced turn-on voltage and enhanced brightness and efficiency which are attributed to the presence of a space charge field near the electrodes caused by the charging of traps[22]. Electrical annealing is done to align the ionic impurities in the presence of an electric field. Due to electrical annealing ionic impurities drift towards organic layer/electrode interface, hence there is large number of traps present near the electrodes. Large trap density near electrodes generates high electric field at interface, which leads to enhancement in charge carrier injection, causing high luminance (nearly 6 times compared to the control device) and device efficiency (nearly 9 times). Improved brightness, low turn-on voltage and higher efficiency have been reported for a solution processed OLED upon electrical annealing[23].

When we apply forward bias on the device, direction of the applied field is opposite to the field associated with the dipoles. Due to this, charge carrier injection is severely diminished and hence there is a decrease in current. However, application of a reverse bias can align the internal field in the direction of the forward bias. Reapplying the same forward bias gives increment in current and luminance because now the resultant field is the sum of the applied field and the internal field[24, 25]. Constant forward biasing causes decay in performance but recovery is possible with reverse bias voltage and subsequently the operating voltage shifts towards lower value for the same brightness[26-28]. This reduction in operating voltage with higher luminance is desirable for the operation of a display unit. In an active matrix (AM) display, using the thin film transistor (TFT) arrays, a very small current is supplied to the OLED in complete time frame[29]. AMOLED can be driven by two ways one is dc mode and the other is ac mode depending upon voltage polarity. Earlier dc mode was considered to be the best option to improve device performance, but bias instability still persisted in the device. So higher amount of reverse bias voltage is applied to the device, which prevents the trapping of space charges in organic layer and de-traps these charges[30]. Thus reverse bias application is helpful in reduction of these trap states and space charge accumulation in OLED can be mitigated.

The effects of thermal annealing and reverse bias thus being established, a combined treatment appears to be worth investigating, also affording an opportunity to study the interaction of the two effects. Annealing under reverse bias conditions has been seen to improve the performance of a polymer-fullerene bulk heterojunction solar cell where improved mobility due to orientation of polymer chains upon annealing has been cited as the reason for the improvement[31]. Similarly, annealing under reverse biased condition has improved the performance of an oligomer-fullerene bulk heterojunction solar cell[32]. Improved performance has been observed upon reverse biased annealing for an organic nanocomposite solar cell. External field is assumed to re-orient the localized dipoles along the direction of the applied field[33]. Burning of shunts and improved mobility of carriers have been cited as the reasons for improved performance in an organic solar cell when subjected to thermal annealing under applied bias[34].

Preferential molecular arrangement has been obtained for pentacene thin films grown by field-assisted deposition[35]. Bajpai et al. have reported a combined electrical and heat treatment on an OLED based on poly (9, 90 dioctylfluorene)-2,7-ylene-ethynylene and showed improved mobility values. This was attributed to dipolar moment[36]. However the change in reverse leakage current has not been reported in this paper.

Thus, to the best of our knowledge, the effect of thermal annealing under reverse bias voltage has not been studied in detail with respect to reverse leakage current in OLEDs. In this paper we have systematically studied the origin of the reverse bias leakage current and devised a simple method to reduce the same in OLEDs.

Results and discussion

The OLED characteristics of a typical device are shown in Fig. 1 and the corresponding current efficiency plot as its inset. The OLED emits in green region and has a current efficiency of 26-28 cd/A in the voltage range of 5-6 V, which indicates a good performance for a fluorescent OLED. The device easily sustains voltages in range 10-15 V, the maximum voltages that are encountered in display drivers, with output luminance in excess of 6000 cd/m^2. However, in applications such as displays, there will be an array of OLEDs and they are accessed through a matrix addressing scheme. This imposes additional performance requirements on reverse leakage current of the diode. For example in a passive matrix display, if the reverse bias current of the OLEDs is high, the leakage current in a display does not allow for its proper addressing. We have successfully fabricated passive matrix OLED displays with materials of the same chemical formula from various sources, that is, with OLEDs having low reverse bias currents[37, 38]. However, the green OLED in this paper suffers from high reverse bias leakage current. This indicates that subtle differences in materials of same chemical formula can lead to significant variations in device performance. Nonetheless, using the OLED reported here as an example, our aim in this work is to demonstrate that even it can be rendered useful by reducing the reverse bias current at the device fabrication stage.

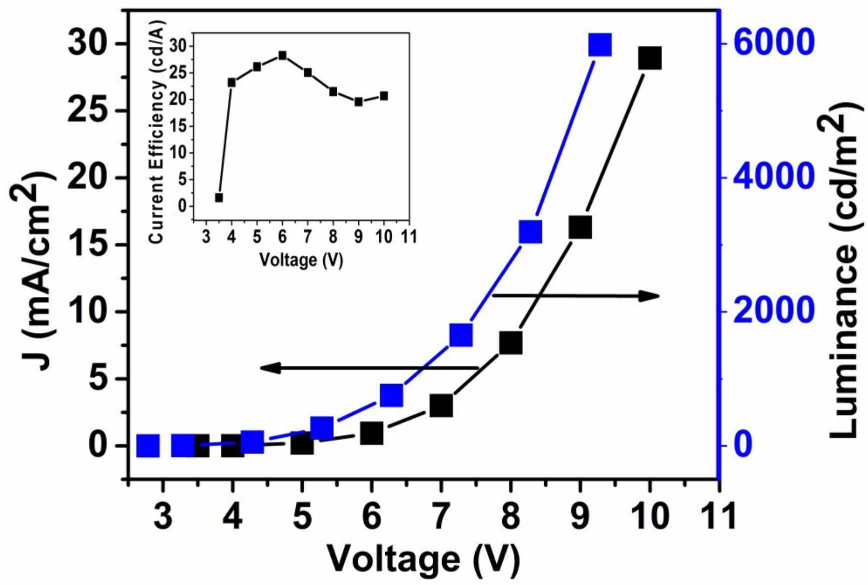

Fig.1 Current – voltage characteristics of green organic light emitting diode

The current-voltage (J-V) characteristics of the green OLED depicted as standard device (case (i)) in Fig. 2 shows high reverse bias current and poor on/off ratio. A well performing OLED in forward bias acts as a diode because in reverse bias the injection barrier for the carriers at the electrodes is very high. In this OLED, clearly injection of carriers has become possible in reverse bias and there is no significant trapping of electrons in m-MTDATA and holes in Alq_3. First, we explore the possibility of reducing the reverse bias current by applying heat, varying subsequent rate of cooling and applying a reverse bias electric field during heating and cooling. Accordingly, following six cases are envisaged:

(i) The OLED as fabricated (standard device), without any thermal annealing.

(ii) Annealing of OLED at 80^{o}C on a hot plate, cooling it off the hot plate, no bias is applied to device

(iii) As in (ii) except reverse bias of -15V is applied during annealing of the device, but not during cooling.

(iv) As in (iii) with reverse bias of -15V is applied during cooling also.

(v) As in (iii), except cooling is carried out on hot plate itself.

(vi) As in (iv), except cooling is carried out on hot plate itself.

All thermal annealing on the hot plate are for 30 minutes duration. The cooling off the hot plate is rapid, taking 3-4 minutes, unlike cooling on the hot plate which takes approximately 90 minutes.

The J-V characteristics of cases (iv) to (vi) are compared in Fig. 2 to that of the standard device (case (i)). The plots for devices (ii) and (iii) are similar to the standard device and, hence, omitted here but provided as Fig. S1 in the supplementary information to avoid cluttering of data. Among the several devices fabricated for each case, the devices compared are those which resulted in lowest reverse bias current; for any of the six cases, the maximum reverse bias current among several samples is clustered in a range of two orders of magnitude. However, the maximum current in the forward biased conditions for all six cases appears in a narrow band (see Fig 2 and supplementary Fig. S1); several samples for any one case are also clustered similarly in a narrow range.

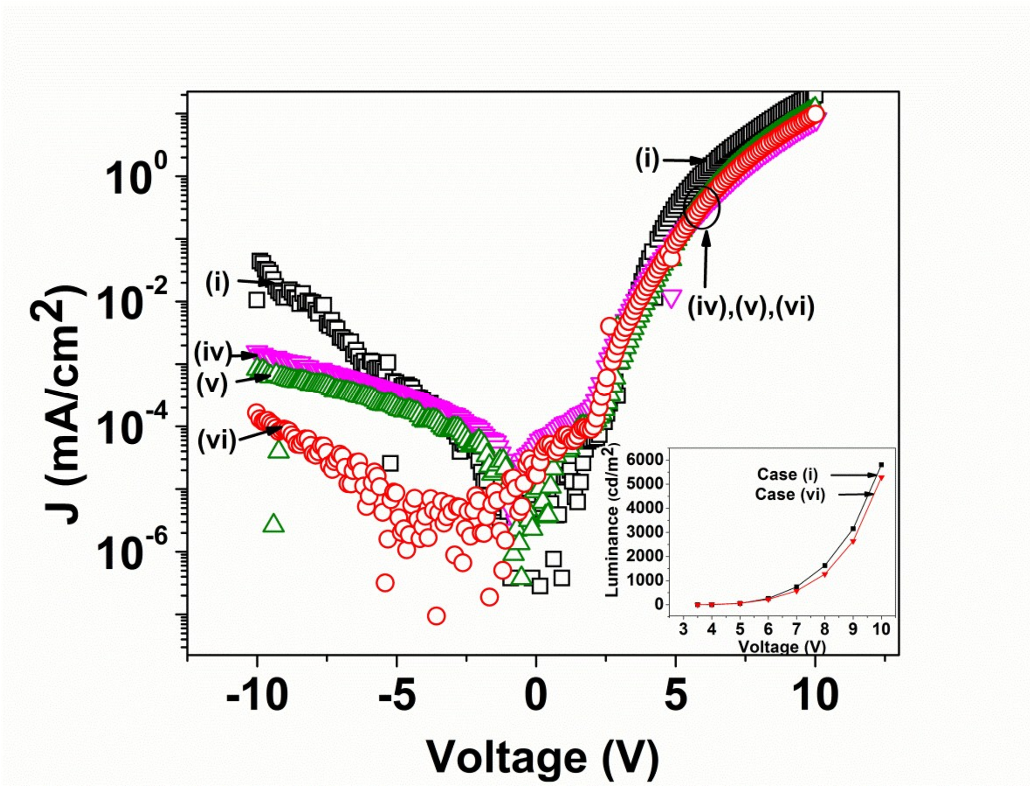

Fig.2 Reduction of reverse bias current with annealing and application of reverse bias voltage; luminance of standard device in forward bias is compared in inset with device after the best annealing treatment.

The various treatments and the corresponding effect on the on/off ratio is presented in Table 1. The annealing of the standard device at 80^{o}C (case ii, in supplementary Fig. S1) has no significant impact on the current characteristics. In some cases, an improved device performance upon annealing was attributed to a flatter and pinhole free morphology and more intimate contact between a m-MTDATA and NPB interface[15]. No improvement in the present case suggests a good morphology and contact in the standard device itself, also corroborated by its high current efficiency. Thus, we also examined whether an applied reverse bias field can play a role in suppressing the reverse bias current and improve the on/off ratio. However, an application of field to the diode during annealing (case iii, supplementary Fig. S1) also does not have much impact. The slope for rise of reverse bias current is high, but its maximum level is still similar to that in the standard device. Hence, it would appear that removal of the field while the device is still warm, that is, during cooling as in case (iii), the reverse bias current recovers back, unlike the result in case (iv), where the field remains applied during cooling too. In this case, while again the forward bias current remains the same as in a standard device, the reverse bias current has reduced by two orders of magnitude. A similar conclusion is drawn by comparing cases (v) and (vi); in both cases the cooling also is on the hot plate, and the field during cooling is applied in case (vi). Further, comparison of cases (iii) and (v) or cases (iv) and (vi) would suggest a slow cooling also assists in reducing the reverse bias current. Hence, in short, we demonstrate that application of a reverse bias field and slow cooling following thermal annealing can reduce the reverse bias current by more than three orders of magnitude and correspondingly improve the on/off ratio to 10^5.

Table 1: Various treatments applied on devices (i) –(vi) and the corresponding values of on/off ratio.

Sample No	Annealing at 80°C	Bias During Annealing	Cooling on Hot Plate	Bias During Cooling	On/off Ratio
i	No	No	No	No	10^2
ii	Yes	No	No	No	10^2
iii	Yes	Yes	No	No	10^2
iv	Yes	Yes	No	Yes	10^3
v	Yes	Yes	Yes	No	10^4
vi	Yes	Yes	Yes	Yes	10^5

It is also important that along with the improvement in the on/off ratio, the luminance from the device does not degrade significantly, which is demonstrated in the inset of Fig. 2, where the green luminance of the standard device is compared with the one annealed under electric field according to the case (vi).

We now examine the cause of reduction in reverse bias leakage current. At the first instance, the OLED structure considered in this work can be thought to act as a diode because of large injection barrier in the reverse bias (meaning aluminum at higher potential than ITO), as indicated through an idealized energy level alignment in Fig. 3, based on data from[39-41].

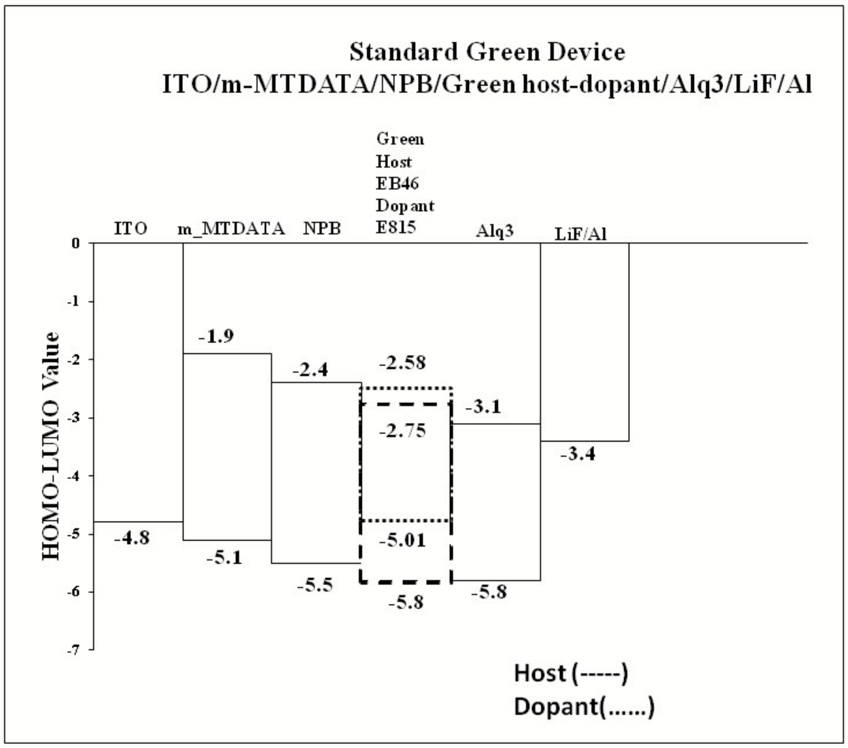

Fig. 3 Energy level alignment in standard OLED

Single layer devices

A large reverse leakage would take place because of either lowered injection barrier for electrons at ITO contact, holes at aluminum contact or carrier tunneling. One possibility for it relates to either presence of trap states in the materials adjacent to the electrodes or the interface states at the metal. Hence, to examine these possibilities, we have fabricated single layer devices with only m-MTDATA or Alq_3. The standard device has a total thickness of organic layers as 195 nm. The single layer m-MTDATA device with the same electrodes is thus having a thickness of 100 nm, the same as in the standard OLED. However, a similar single layer Alq_3 with the same thickness as in the standard OLED is too thin and leads to electrical shorts. Therefore, the single layer Alq_3 device is also fabricated with a thickness of 100 nm. The current-voltage characteristics of these diodes are measured both before annealing and after annealing according to case (vi); henceforth all annealing treatments to the device conform to case (vi).

We first examine the m-MTDATA device. According to the idealized band alignments for such device the forward biased current should be hole dominated. In Fig. 4(a), the forward current in this device is high. Even after accounting for the fact that this device is of approximately half the thickness of a standard device, the current is still higher in comparison to the standard device (case (i)). The work function of LiF coated Al is reported to be approximately 3.4 eV[42]. However, use of LiF is shown to provide good contacts to even m-MTDATA or NPB[43]. Hence, it is possible that in forward bias, there is also an electron current, thus leading to this large current. The reverse biased current is approximately 3 orders of magnitude lower. This ratio is similar to that for a standard device, case (i). However, when the m-MTDATA device is annealed under bias, both forward and reverse currents reduce by similar magnitude, that is, the full J-V curve shifts down in current. This is unlike the standard device, where when we compare case (i) and (vi) the forward current does not change but the reverse bias current is significantly reduced. Hence, we carry out a similar examination of the Alq_3 device.

The forward current in Alq_3 device is also high (see Fig. 4(b)). But in this device, when it is annealed, the forward biased current does not change, while the reverse bias current decreases significantly. Thus, this device behaves similar to the standard device.

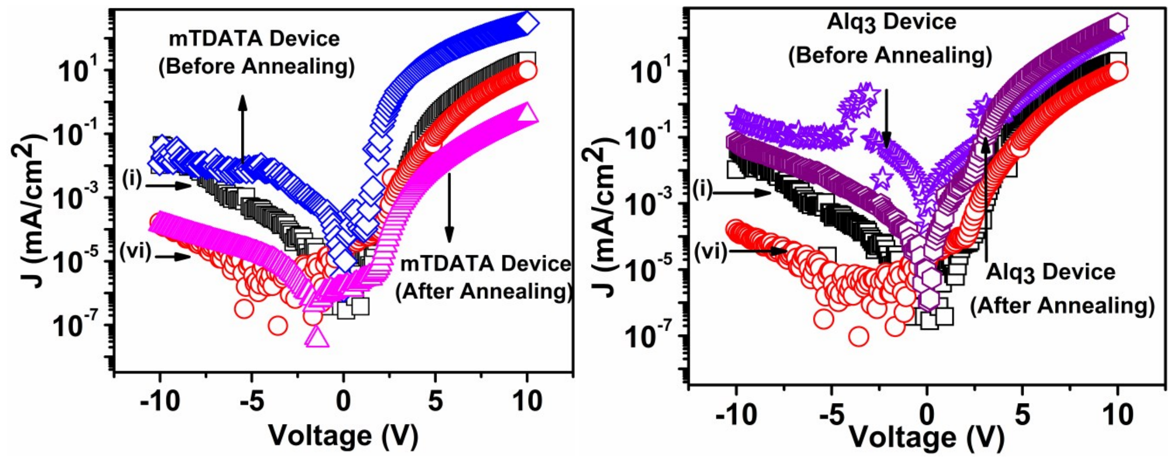

(a) (b)

Fig. 4 Current-voltage characteristics of single layer (a) m-MTDATA and (b) Alq_3 before and after annealing are compared with case (i) and (vi) of standard device.

Hence, it would appear that the origin of improved on/off ratio after annealing in the standard device has its origin in changes in Alq_3 layer. It has been earlier reported that with annealing, the electron only device alone showed improved performance[12]. However, since m-MTDATA device also exhibited overall lowering of current, further examination is necessary.

Therefore, next we estimate the changes in trap densities operative under reverse bias before and after annealing of both m-MTDATA and Alq_3 devices. Then we also evaluate the effective barrier heights for injection for these two devices.

Trap densities in single layer devices

Under reverse bias, electrons are injected in m-MTDATA and holes in Alq_3. Thus, we are estimating the nature of electron and hole traps in m-MTDATA and Alq_3, respectively. As it is common, we approximate the traps to be distributed exponentially. Accordingly, the trap distribution in energy, H(E) is given by $H_t/E_t \exp[(E-E_{LUMO})/E_t]$ for m-MTDATA or $H_t/E_t \exp[(E_{HOMO}-E)/E_t]$ for Alq_3, where H_t, E_t, E_{HOMO} and E_{LUMO} are total trap density, characteristic energy of the exponential distribution, HOMO and LUMO levels, respectively[44, 45]. As an approximation, the trap limited current is given by

$$J = K\left(\frac{V^{m+1}}{d^{2m+1}}\right) \quad (1)$$

where

$$K = \mu N_o q^{(1-m)} \left(\frac{(2m+1)}{(m+1)}\right)^{(m+1)} \left(\frac{\varepsilon m}{(m+1)H_t}\right)^{m} \quad (2)$$

And $m=E_t/kT$. Here, μ and N_o are carrier mobility and effective density of states of the band relevant to the carrier, respectively, and d, Ɛ and q are thickness, permittivity and fundamental charge, respectively.

In order to determine the trap densities, we measure the current-voltage characteristics of both single layer devices at several low temperatures. In Fig. 5, such measurement for m-MTDATA device before and after annealing (according to case (vi)) is provided and the object is to estimate the change in the trap density. We focus only at higher voltages (-5 to -10 V) in the reverse bias conditions, and proceed in a manner similar to Campbell et al.[46]. From the slope and intercept of log(J) and log(V) curve, based on eq. (1), first m and K/d^{2m+1} are determined at each temperature. A separate plot using dielectric constant of organic layers as 3 is generated from eq. (2) for an assumed value (discussed later) of μN_o as solid lines in Fig. 6. For the range of data we are interested in, straight lines are obtained with slope that depends on the value of trap density. Changing μN_o simply raises or lowers the lines up and down. Therefore, it is possible to superimpose the measured data (extracted values of m and K/d^{2m+1} through eq. (1)), points on Fig. 6, and change μN_o until one of the lines matches the data points, allowing estimate of both μN_o and H_t.

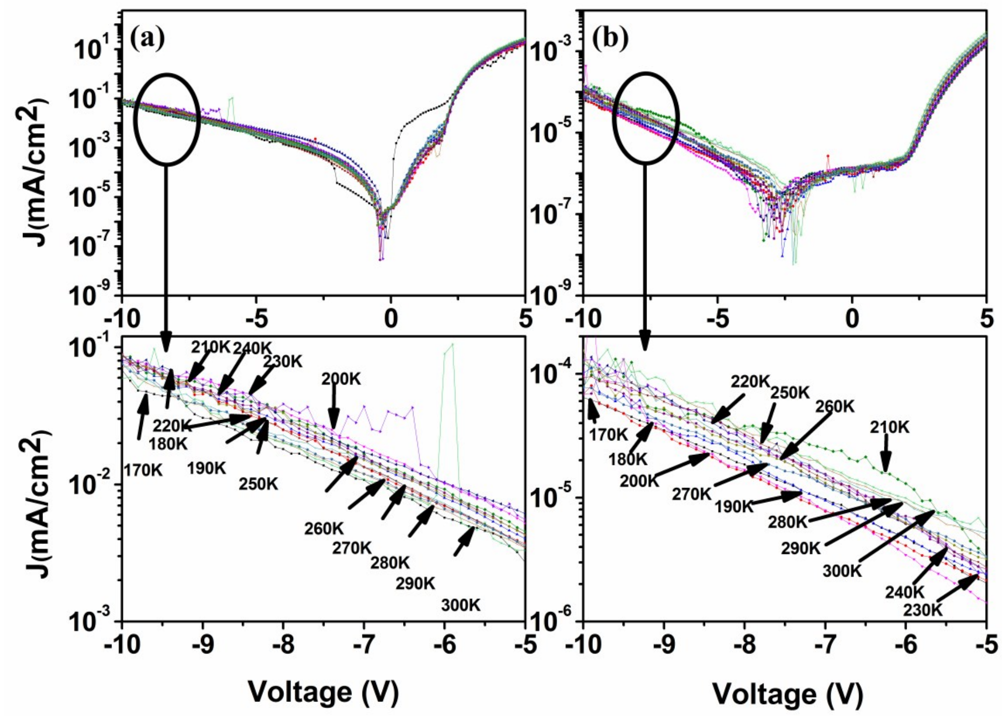

Fig.5 Current-Voltage measurement at various temperatures for single layer m-MTDATA device (a) before annealing and (b) after annealing

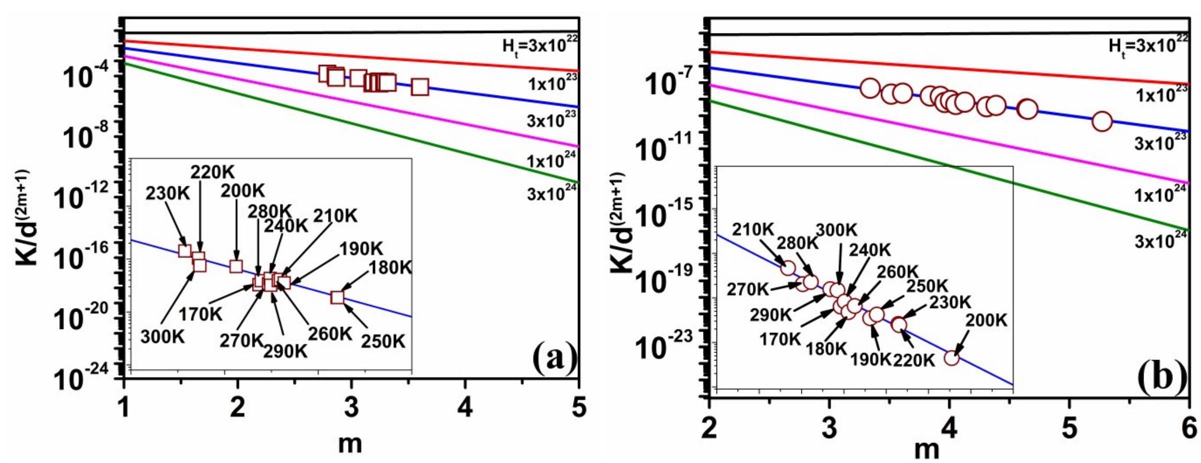

Fig.6. Variation of $K/d^{(2m+1)}$ with m to find the trap density in m-MTDATA device at various temperatures (a) before annealing and (b) after annealing. The inset gives the different temperature values corresponding to the measured points (all quantities in SI units)

Accordingly, for the single layer m-MTDATA device, we have determined μN_o and trap density H_t for electron traps to be $7x10^{10}$ $m^{-1}V^{-1}s^{-1}$ and $3x10^{23}$ m^{-3}, respectively, before annealing and $8x10^{7}$ $m^{-1}V^{-1}s^{-1}$ and $3x10^{23}$ m^{-3}, respectively, after annealing. This would suggest no change in trap density but likely reduction of electron mobility in m-MTDATA upon annealing. However, such conclusion would be erroneous. Since, such analysis is common, the purpose of including this discussion, in spite of being erroneous, is to highlight that if care is not taken in analysis according to[46], then wrong conclusions may be drawn.

When the data fits the analysis as above, it should also follow the analysis according to Kumar et al.[47], where from a crossover voltage in log-log plot of J and V, the trap density is determined. However, the present data does not exhibit a crossover voltage. A closer examination of insets in Fig. 6 reveals the temperature values corresponding to the measured data points. The analysis would be accurate only if values of m decrease as T increases. However, that is not the case, because under reverse bias of -5 to -10 V, the current values, shown in inset of Fig. 5 appear in a band with slopes in no fixed pattern with respect to the temperature. That is, all currents values at any voltage in this specific range are similar, unaffected by temperature. The data for single layer Alq_3 device also suffers from a similar infirmity and hence is not reproduced here, but provided in Fig.S2 in the supplementary information. Hence, because of the nature of the reverse bias currents at various temperatures, it cannot be said that the current is trap limited in both these devices. Thus, native electron traps in m-MTDATA or hole traps in Alq_3 bulk do not seem to provide intermediate states near the electrode for carriers injection during reverse bias.

Further, because increase in current during reverse bias with increasing temperature is non-exponential as evident from Fig. 5 (and similarly for Alq_3 device), we also rule out thermionic injection into the band states.

Hence, the other possibility is carrier injection by tunneling into states that may form at the interface with or adjacent to the metal electrodes, presenting a low effective barrier height for injection. Thus, we also investigate tunneling injection.

Tunneling Injection

In tunneling injection, explicit forms of J-V relations are available in specific instances, for example, for trapezoidal and triangular barriers[48]. In our case, the trapezoidal barrier is unlikely due to significant thickness of the transport layer. Further, such barrier leads to a linear J-V relationship, which is not seen here. Alternatively, for a triangular barrier

$$\ln\left(\frac{J}{V^2}\right) = -\left(\frac{1}{V}\right)\left(\frac{4t\sqrt{2m^*\emptyset_B^3}}{3\hbar q}\right) + \text{constant} \qquad (3)$$

where m* is effective mass of the charge carrier. The two quantities t and $\emptyset_B$ are referred to as thickness and barrier height, but these are enunciated better shortly. In Fig. 7, $\log(J/V^2)$ is plotted against 1/V for the Alq_3 device. Before annealing, the R^2 value indicates uncorrelated $\log(J/V^2)$ with 1/V before annealing, whereas a small correlation is seen after the device is annealed. Hence, before annealing, as J/V^2 is independent of voltage (a constant), there appears to be no barrier to injection, but a small one appears after annealing. Estimating that small barrier from the slope may be meaningless in absence of known value for m* or effective value of t. The plot of log(J/V2) vs. 1/V for the m-MTDATA device is given as Fig.S3 in the electronic supplementary information. The m-MTDATA device also exhibits a similar pattern.

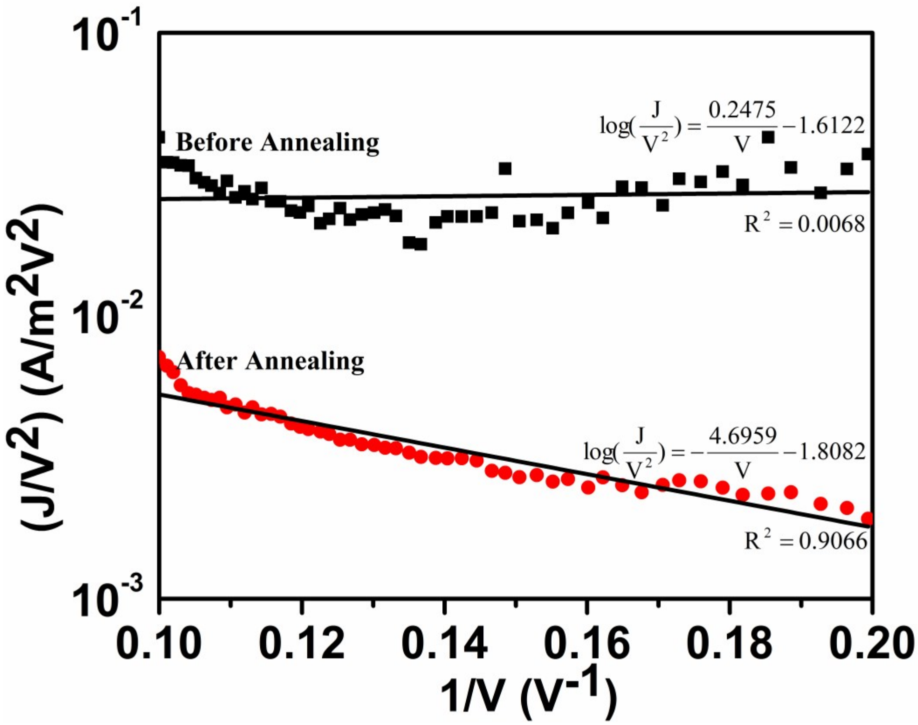

Fig.7 Fit for tunneling injection in Alq_3 single layer device before and after annealing.

Hence, putting together all these observations, that:

(a) When a single layer Alq_3 device is annealed, the forward current remains the same before and after annealing, while the reverse current is significantly decreased upon annealing. However, in m-MTDATA single layer device both forward and reverse current are impacted upon annealing. The behavior of the Alq_3 device is similar to that of the OLED device, which may suggest Alq_3 layer is the cause of observed behavior in the OLED device.

(b) The reverse bias current does not appear to be trap limited, and hence availability of mid-gap states due to native traps of the materials for injection at the electrode is not expected.

(c) The reverse bias current is not due to thermionic reasons.

The schematic in Fig. 8 may explain the injection behavior in the OLED device. There are available states for hole injection at the Alq_3/cathode interface, distributed between the HOMO-LUMO gap. Before annealing, the hole states are aligned close to the electrode Fermi-level even in thermal equilibrium and hence the same states are accessible even upon reverse bias. Accordingly, $\log(J/V^2)$ and $1/V$ remain uncorrelated because the tunneling is in absence of a barrier. But, upon annealing, the hole states reduce in width and the first available state for injection has a barrier, though it is still smaller than that to the HOMO level. Hence, the thickness t relevant to this picture is that between the electrode and the adjacent layer containing these energy levels. The leakage in reverse bias is now smaller because injection requires a greater field to bring the available states in alignment with the cathode level.

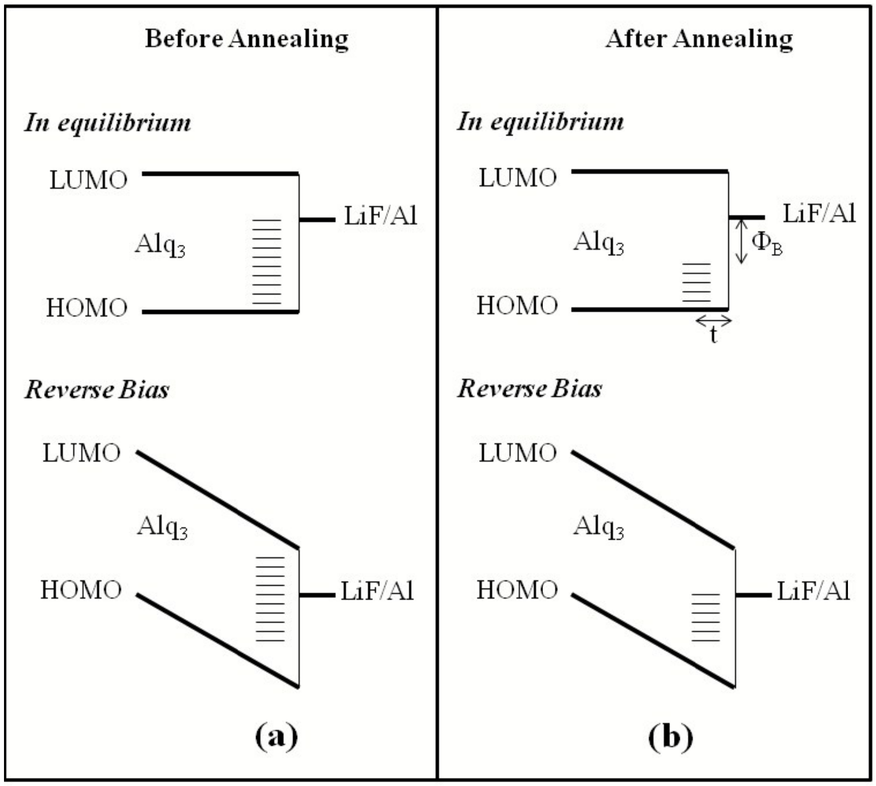

Fig.8 Schematic diagram showing elimination of deep hole traps on annealing the Alq_3 device under electric field. (a) Before annealing, a hole state is available for injection, (b) but it becomes available after annealing, only when a much higher reverse bias is applied.

In summary, the likely cause of reduction of leakage current in the OLED device upon annealing under electric field is the elimination of deep hole traps at or near Alq_3/cathode interface. The damage of the interface caused by thermal evaporation may facilitate injection of holes into these traps, as also suggested by the fact when devices in which cathode was deposited at 77K had much lower reverse leakage current[10]. Furthermore, the electronic states in a material or device change along with morphology upon annealing or application of electric field. This aspect we have reviewed earlier along with our results for pentacene[35]. In the present case, since the electrodes are in intimate contact with the organic material, morphological imaging is difficult.

However, along those lines we believe that the combined electrical and heat treatment is repairing the damage along with a morphological evolution and thus correcting the energetics so as to prevent hole injection from the cathode which leads to the reverse leakage current.

Conclusions

Previously, both annealing and application of electric field individually have been used to improve the quality of thin layers in OLED during the device fabrication stage or even after fabrication of the device to improve its performance. In the present work, we have systematically investigated the role of both and shown that application of electric field in reverse bias during annealing itself is the best option. Specifically, annealing of the device under reverse bias condition and then cooling it slowly while retaining the field during cooling works the best. In this study, the focus is on suppressing the reverse bias leakage current, without adversely affecting the forward bias current or the light emission. Thus, the paper presents a method that can potentially be used when reverse bias J-V characteristics are poor for a given batch or source of materials.

The cause of reduction in reverse bias leakage current and corresponding improvement in On/Off ratio of the diode was also investigated. The likely reason appears to be reduction in deep hole states at or near the Alq_3/cathode interface.

Experimental section

In this study all the devices were fabricated on glass substrates pre-coated with indium tin oxide (ITO), which acts as anode. ITO coated substrates were then cleaned with detergent solution, thoroughly rinsed in de-ionized water and acetone respectively. For removal of organic and inorganic contaminants cleaning of the substrates was done with the well known RCA (Radio

Corporation of America) solution. Prior to deposition of organic layers these cleaned ITO substrates were treated with oxygen-argon plasma. After plasma treatment, organic layers were deposited using thermal evaporator under ultra high vacuum of the order of 10^{-8}Torr at room temperature. A hole injecting layer (HIL) 4,4',4''-Tris(N-3-methylphenyl-N-phenylamino)triphenylamine (m-MTDATA) was deposited followed by hole transport layer (HTL) N,N′- di(1-naphthyl)-N,N′-diphenyl-(1,1′-biphenyl)-4,4′-diamine (NPB), green host EB-46, green dopant EB-815 and electron injecting layer (ETL) Tris-(8-hydroxyquinoline)aluminum (Alq_3). After deposition of the organic layers LiF and Al were deposited as a cathode followed by encapsulation of the devices with UV-curable epoxy. For experimental studies we have fabricated three different type of devices (a) green OLED with structure, also labeled as a standard device, ITO/ m-MTDATA (100 nm) /NPB (25 nm) /green host EB-46 (30 nm) / green dopant E-815 (1.5 nm) /Alq_3 (25 nm) /LiF (8 nm) /Al (200 nm) (b) single HIL layer device ITO/ m-MTDATA (100 nm)/ LiF (8 nm) /Al (200 nm) and (c) single ETL layer device ITO/ Alq_3 (100 nm) /LiF (8 nm) /Al (200 nm). All of the HIL, HTL, ETL were deposited with a highly precise rate of 1 Å/s. Green host and green dopant were deposited with rates 1 Å/s and 0.05 Å/s respectively. The HIL, HTL and ETL are from Sensient Technologies, USA and others from e-Ray Optoelectronics Technology Company Ltd, Taiwan.

References

1. M. Pope, H. P. Kallmann and P. Magnante, *J. Chem. Phys.*, 1963, **38**, 2042-2043.
2. S. Reineke, F. Lindner, G. Schwartz, N. Seidler, K. Walzer, B. Lussem and K. Leo, *Nature*, 2009, **459**, 234-238.
3. R. Singh, K. N. N. Unni, A. Solanki and Deepak, *Opt. Mater.*, 2012, **34**, 716-723.
4. G. Gu and S. R. Forrest, *IEEE J. Sel. Topics Quantum Electron.*, 1998, **4**, 83-99.
5. K.B. Kim, Y.H. Tak, H.G. Park, K.H. Lee and J.R. Lee, *MRS Online Proceedings Library*, 2001, **708**.
6. K. Long, *Ph.D. Thesis, Princeton University*, 2006.
7. G. G. Belmonte, J. M. Montero, Y. A. Limonge, E. M. Barea, J. Bisquert and H. J. Bolink, *Curr. Appl. Phys.*, 2009, **9**, 414-416.

8. X. N. Xie, J. Wang, K. P. Loh and A. T. S. Wee, *Appl. Phys. Lett.*, 2009, **95**, 203302.
9. S. Nowy, W. Ren, J. Wagner, J. A. Weber, and W. Brutting, *Proc. SPIE*, 2009, **7415**, 74150G-74151.
10. B. H. Chu, B. D. Chin, K. H. Baik, S. J. Pearton, F. Ren and S. Jang, *Jpn. J. Appl. Phys.*, 2012, **51**, 09MH04.
11. E. J. Miller, E. T. Yu, P. Waltereit and J. S. Speck, *Appl. Phys. Lett.*, 2004, **84**, 535-537.
12. M. Ishihara, K. Okumoto and Y. Shirota, *J. Photopolym. Sci. Tech.*, 2002, **15**, 769-773.
13. M. C. Sun, J. H. Jou, W. K. Weng and Y. S. Huang, *Thin Solid Films*, 2005, **491**, 260-263.
14. J. X. Sun, X. L. Zhu, X. M. Yu, H. J. Peng, M. Wong and H. S. Kwok, *J. Display Technol.*, 2006, **2**, 138-142.
15. G.T. Chen, S.H. Su, C.C. Hou and M. Yokoyama, *J. Electrochem. Society*, 2007, **154**, J159.
16. S. Sepeai, M. M. Salleh, M. Yahaya and A. A. Umar, *Thin Solid Films*, 2009, **517**, 4679-4683.
17. K. Jokinen, A. Bykov, R. Sliz, K. Remes, T. Fabritius and R. Myllylä, *Solid State Electron.*, 2015, **103**, 184-189.
18. J. H. Ahn, C. Wang, N. E. Widdowson, C. Pearson, M. R. Bryce and M. C. Petty, *J. Appl. Phys.*, 2005, **98**, 054508.
19. S. Caria, E. D. Como, M. Murgia, R. Zamboni, P. Melpignano and V. Biondo, *J. Phys.: Condens. Mat.*, 2006, **18**, S2139-S2147.
20. Y. Yoon, H. Lee, T. Kim, K. Kim, S. Choi, H. K. Yoo, B. Friedman and K. Lee, *Solid State Electron.*, 2013, **79**, 45-49.
21. D. S. Qin, D. C. Li, Y. Wang, J. D. Zhang, Z. Y. Xie, G. Wang, L. X. Wang and D. H. Yan, *Appl. Phys. Lett.*, 2001, **78**, 437-439.
22. D. Ma, J. M. Lupton, R Beavington, P. L. Burn and I. D. W. Samuel, *J. Phys. D: Appl. Phys.*, 2002, **35**, 520-523.
23. B. Park, C. H. Park, Y. Yim and J. Park, *J. Appl. Phys.*, 2010, **108**, 084508.
24. D. Zou, M. Yahiro and T. Tsutsui, *Synthetic Met.*, 1997, **91**, 191-193.
25. H. Jeong, D. Zou, T. Tsutsui and C. S. Ha, *Thin Solid Films*, 2000, **363**, 279-281.
26. D. Zou, M. Yahiro and T. Tsutsui, *Appl. Phys. Lett.*, 1998, **72**, 2484-2486.
27. D. Zou, M. Yahiro and T. Tsutsui, *Jpn. J. Appl. Phys.*, 1998, **37**, L1406-L1408.
28. D. Zou and T. Tsutsui, *J. Appl. Phys.*, 2000, **87**, 1951-1956.
29. Y. Si, L. Lang, Y. Zhao, X. Chen and S.Liu, *IEEE Trans. Circuits Syst. II: Exp. Briefs,* 2005, **52**, 856-859.
30. S. A. Van Slyke, C. H. Chen and C. W. Tang, *Appl. Phys. Lett*, 1996, **69**, 2160-2162.
31. Y. Li, Y. Hou, Y. Wang, Z. Feng, B. Feng, L. Qin and F. Teng, *Synthetic Met.*, 2008, **158**, 190-193.
32. S. Alem, A. K. Pandey, K. N. N. Unni, J. -M. Nunzi and P. Blanchard, *J. Vac. Sci. Technol. A*, 2006, **24**, 645-648.
33. Ajay K. Pandey, H.Wang, C.C. Oey, A.B. Djurisic, M.H. Xie, Y.H. Leung, K.K.Y. Man, W.K. Chan, P.C. Chui and J.M. Nunzi, *Nonlin.Opt. Qtm. Opt*, **37**, 123-131.
34. F. Padinger, R. S. Rittberger and N. S. Sariciftci, *Adv. Funct. Mater.*, 2003, **13**, 85-88.
35. T. Mandal, A. Garg and Deepak, *J. Appl. Phys.*, 2013, **114**, 154517.
36. M. Bajpai, R. Srivastava, M. N. Kamalasanan, R. S. Tiwari and S. Chand, *J. Appl. Phys.*, 2011, **109**, 084512.
37. P. K. Uttwani, B. C. Villari, K. N. N. Unni, R. Singh, A. Awasthi and Deepak, *J. Display Technol.*, 2012, **8**, 154-161.
38. Deepak, International Workshop on Physics of Semiconductor Devices, IWPSD, 2007.
39. Sensient Imaging Technologies GmbH, OLED sales products.
40. http://www.eray-tech.com/products_content.php?v=1&c=59.
41. http://www.eray-tech.com/products_content.php?v=1&c=218.
42. R. Schlaf, B. A. Parkinson, P. A. Lee, K. W. Nebesny, G. Jabbour, B. Kippelen, N. Peyghambarian and N. R. Armstrong, *J. Appl. Phys.*, 1998, **84**, 6729-6736.

43. D. Li, G. Dong, L. Duan, L. Wang and Y. Qiu, *J. Phys. Chem. C*, 2012, **116**, 5235-5239.
44. A. Rose, *Physical Review*, 1955, **97**, 1538-1544.
45. P. Mark and W. Helfrich, *J. Appl. Phys.*, 1962, **33**, 205-215.
46. A. J. Campbell, D. D. C. Bradley and D. G. Lidzey, *J. Appl. Phys.*, 1997, **82**, 6326-6342.
47. V. Kumar, S. C. Jain, A. K. Kapoor, J. Poortmans and R. Mertens, *J. Appl. Phys.*, 2003, **94**, 1283-1285.
48. B. K. Sarker and S. I. Khondaker, *ACS Nano*, 2012, **6**, 4993-4999.